



OPEN

A reliable prognostic model for hepatocellular carcinoma using neutrophil extracellular traps and immune related genes

Defeng Yuan^{1,5}, Feng Zhang^{2,5}, Pengfei Lv^{1,5}, Jun Zhu^{3,5}, Haiwei Zhang^{1,5} & Zhengcong Zhang^{1,4}✉

Neutrophil extracellular traps (NETs) and immunity play critical roles in liver hepatocellular carcinoma (LIHC) progression, but their mechanisms remain unclear. This study explored the potential of NETs-related genes (NETs-RGs) and immune-related genes (IRGs) as prognostic markers for LIHC. LIHC transcriptome data and IRGs were obtained from public databases, and NETs-RGs were derived from prior research. Differentially expressed genes (DEGs) intersecting with key module genes were identified, followed by Cox regression analysis and machine learning to determine prognostic genes. A risk prediction model and nomogram were constructed and validated. Enrichment analysis, immune infiltration, and drug sensitivity studies were conducted to explore underlying mechanisms. Reverse transcription quantitative PCR (RT-qPCR) was used to validate findings. Five prognostic genes—*HMOX1*, *MMP9*, *TNFRSF4*, *MMP12*, and *FLT3*—were identified. A risk model and nomogram demonstrated strong predictive ability. Gene set enrichment analysis revealed pathways related to retinol metabolism and cytochrome P450 drug metabolism in different risk groups. Immune infiltration analysis showed regulatory T cells positively correlated with MDSCs, which were directly associated with the five genes. Drug sensitivity analysis identified 74 drugs with differential sensitivity between risk groups; axitinib showed lower sensitivity in high-risk patients, while ABT-888 showed higher sensitivity. RT-qPCR confirmed reduced *HMOX1* and *FLT3* expression in LIHC tissues, while *MMP9* and *TNFRSF4* were upregulated. This study developed a robust predictive model for LIHC prognosis, offering valuable insights for clinical management and personalized treatment strategies.

Keywords Hepatocellular carcinoma, Neutrophil extracellular traps, Immunity, Prognostic gene

Hepatocellular carcinoma (HCC), the prevalent sub-type of liver cancer and the fourth leading cause of cancer-related mortality globally, often impacts individuals suffering from chronic liver disease and cirrhosis¹. Consequently, it claims the dubious distinction of being one of the deadliest cancers globally². Illnesses commonly arise from viral hepatitis infections, chronic liver conditions, alcohol abuse, and metabolic disorders such as diabetes³. Although patients can be cured by liver transplantation, surgical resection and thermal ablation, long-term outcomes are compromised by high recurrence rates (up to 70% of cases 5 years after treatment)⁴. Clinical statistics reveal that a significant number of patients are often diagnosed at advanced stage, resulting in the inability to achieve a complete cure⁵. Even though multiple biomarkers for HCC have been identified to aid in surveillance and early detection, there are still a considerable proportion of individuals with poor survival^{6,7}. Therefore, it is crucial to investigate new therapeutic targets to improve the treatment efficacy of HCC.

Research suggest that rapid progression of HCC and poor survival rates are frequently attributed to the presence of heterogeneous sub-populations of tumor cells⁸.

A key factor influencing the heterogeneity of HCC is the tumor micro-environment (TME)⁹. Inflammation in the liver micro-environment plays a pivotal role in cancer invasion and metastasis, and pro-inflammatory

¹The eleventh Ward of General Surgery, The First Hospital of Lanzhou University, Lanzhou 730000, Gansu Province, China. ²The third ward of Medical Oncology, The First Hospital of Lanzhou University, Lanzhou 730000, Gansu Province, China. ³Department of Pathology, The First Hospital of Lanzhou University, Donggang District, Lanzhou 730000, Gansu Province, China. ⁴The First Clinical Medical College of Lanzhou University, Lanzhou 730000, Gansu Province, China. ⁵Defeng Yuan, Feng Zhang, Pengfei Lv, Jun Zhu and Haiwei Zhang contributed equally to this work. ✉email: 120220903471@lzu.edu.cn

cytokines secreted by immune cells implicated in steatohepatitis can also promote cancer progression¹⁰. Neutrophils, as the most numerous type of white blood cells in human immune system, play a complex and important role in the TME¹¹. Studies have shown that the accumulation of tumor-associated neutrophils (TANs) in tumors can be triggered by external stimuli from TME, leading to a switch between pro-tumor and anti-tumor phenotypes¹².

Neutrophil extracellular traps (NETs) are web-like structures released by activated neutrophils, primarily composed of decondensed chromatin and intracellular granule proteins¹³. Initially, it was discovered to capture and eliminate extracellular pathogens, playing a protective role in antibacterial defense¹⁴. Tumor-associated neutrophils have been shown to readily form NETs in HCC, indicating that NETs play a significant role in the progression and metastasis of liver cancer¹⁵. Zhan et al.'s mechanistic study revealed that the levels of NETs are markedly increased in hepatitis B virus (HBV)-positive HCC. Suppressing NETs via the TLR4/RAGE-ROS signaling pathway could potentially be advantageous for HCC patients¹⁶. Additionally, studies have found that NETs trigger tumorous inflammatory response and fuel HCC metastasis. Focusing on NETs, rather than the neutrophils directly, may present a viable strategy to combat HCC metastasis¹⁷. One study also proved that NETs can effectively predict the immunotherapy response and prognosis of HCC patients as imaging genomics biomarkers¹⁸. Therefore, analyzing the levels of NETs and their relationship with the survival of HCC patients is of great value. Moreover, the new and reliable prognostic model developed by NETs offers enhanced guidance for targeted therapy.

This study aims to identify prognostic genes associated with NETs through TCGA database, and to explore the correlation between NETs and TME. Thereafter, the nomograms were constructed using the prognostic genes. Studies on enrichment analysis, immune infiltration, and drug sensitivity provides a deeper understanding of the complex mechanisms of these prognostic genes. The ultimate aim is to offer potential guidance for targeted and immunotherapeutic treatments of HCC, as well as to provide fresh perspectives for prognostic evaluations.

Materials and methods

Data source

TCGA-HCC was downloaded on August 19, 2024, from the cancer genome atlas (TCGA, <https://portal.gdc.cancer.gov>), contained 374 LIHC tissue samples and 50 adjacent tissue samples (control cohort), among which existed 368 tumor tissue samples with survival information. The validation cohort GSE14520 (GPL3921) tracked to gene expression omnibus (GEO, <https://www.ncbi.nlm.nih.gov/geo/>) database, including 221 LIHC tumor samples with survival information. The count and FPKM data from TCGA were logarithmically transformed (using $2^x - 1$ and $\log_2(x + 1)$) to compress the data range. Additionally, the data were further standardized using the Z-score normalization method, so that the mean of the data became 0 and the standard deviation was 1.

The na.omit function was directly used to delete the rows containing missing values. If the data information was not desired to be lost, the mean imputation method could be employed, that is, the missing values were replaced with the mean value of the corresponding column. The quality of the data and the pertinence of the analysis were ensured by removing the duplicate gene information and screening the samples according to the sample types. From a previous study¹⁹, a total of 87 neutrophil extracellular traps-related genes (NETs-RGs) were obtained. Referring to the methods of a previous study²⁰, 1793 immune-related genes (IRGs) were acquired.

Differentially expressed genes (DEGs) identification

DESeq2 package (v 1.38.0)²¹ was engaged to pinpoint DEGs between cancerous and control tissues samples with survival information in the TCGA-LIHC ($p_{\text{adj}} < 0.05$ and $|\log_2 \text{fold change (FC)}| > 1$). Subsequently, ggplot2 package (v 3.4.1)²² was applied to create a volcano plot of DEGs, while the top 10 up-regulated and down-regulated DEGs were annotation in volcano plot ranked by $|\log_2 \text{FC}|$. Furthermore, we utilized the ComplexHeatmap package (v 2.14.0)²³ to generate a heatmap for these 20 DEGs.

Weighted gene co-expression network analysis (WGCNA)

First, a preliminary gene screening of NETs-RGs was conducted via univariate Cox regression ($p < 0.05$). Subsequently, we calculated the NETs-RGs scores for both the tumor cohort with survival information and the normal cohort in TCGA-LIHC using ssGSEA algorithm from GSVA package (v 1.42.0)²⁴. Then, differences between the two cohorts were tested ($p < 0.05$). After that, 368 LIHC patients were cohorted via median NETs-RGs score and a survival analysis utilizing the Kaplan-Meier (K-M) was performed on the two cohorts with the aid of the survival package (v 3.5.3)²⁵ ($p < 0.05$).

Next, in all samples of the TCGA-LIHC dataset, WGCNA analysis was completed through WGCNA package (v 1.7.1)²⁶. Initially, LIHC samples were clustered to identify and remove outliers. PckSoftThreshold was employed to determine the soft value required to construct the scale-free network ($R^2 = 0.85$). Subsequently, a hierarchical clustering dendrogram was constructed using a dynamic tree cut method ($\text{minModuleSize} = 500$). Finally, by calculating the correlation coefficient matrix and p-values between gene modules and NETs-RGs scores, we selected the modules most correlated with NETs-RGs scores ($|\text{correlation (cor)}| > 0.3$ and $p < 0.05$), the module genes were named key module genes.

Pinpointed candidate genes and function enrichment evaluation

Candidate genes were obtained through DEGs, IRGs and key module genes by ggvenn package (v 0.1.9). Subsequently, the clusterProfiler package (v 4.7.1.3)²⁷ was utilized to perform gene ontology (GO) and kyoto encyclopedia of genes and genomes (KEGG) to research the potential pathways and functions of these candidate genes ($p_{\text{adj}} < 0.05$)^{28–30}. An the enrichment results were sorted in ascending order by p.adj value, displaying the top 10 most significant functions; for KEGG, the top 5 most significant pathways were displayed. Then,

a protein-protein interaction (PPI) network was generated by STRING (<https://string-db.org/>) (interaction score > 0.4) to gain insights into the interconnections between these genes and was visualized using Cytoscape (v 3.5.2), and genes with interactions were retained for further analysis.

Construction and validation of prognostic models

To further screen for genes with prognostic value from the candidate genes, we first took the following steps in TCGA-HCC: univariate Cox regression analysis (hazard ratio (HR) $\neq 1$ and $p < 0.05$) and proportional hazards (PH) assumption test ($p > 0.05$) were performed via survival package. A HR value greater than 1 indicated that the gene was a risk gene for CC, an HR value less than 1 indicated that the gene was a protective gene for HCC, and an HR value of 1 indicated that the result was meaningless. Meanwhile, the 95% confidence interval (CI) values were calculated. Least absolute shrinkage and selection operator (LASSO) was used to select prognostic genes, which was accomplished by glmnet package (v 4.1.4)³¹. The LASSO analysis, through 10-fold cross-validation, could compress the regression coefficients of some unimportant variables to 0, thus achieving variable selection. In traditional regression methods, when dealing with multicollinearity, the estimated regression coefficients were unstable, and the standard errors were increased, resulting in inaccurate judgments of the significance of variables. The regularization feature of LASSO could make the coefficients of some of the independent variables with collinearity become 0, and only one or a few independent variables that had a greater impact on the dependent variable were retained. In this way, the problem of multicollinearity was effectively alleviated, and the stability of the model was improved³². Then, the Bootstrap method was used to evaluate the reliability of the model. Each gene in the model was sampled 1000 times with replacement. After each sampling, the Cox regression model was fitted, and the regression coefficients were recorded. Finally, the mean value, standard deviation, and 95% confidence interval of the regression coefficients for each gene were calculated. For small samples, the exact Cox regression was used instead of the asymptotic Cox regression, which could estimate the parameters and test the hypotheses more accurately. In order to ensure that the model was not overfitted and that sufficient statistical power was maintained when the sample size was small, the exact Cox regression was used instead of the asymptotic Cox regression for small samples, as it could estimate the parameters and test the hypotheses more accurately. After that, a predictive risk model was established by integrating these selected prognostic genes. The methodology for determining the risk score is outlined follow: risk score = $\sum_{j=1}^n \text{Expr}(\text{gene}_j) \times \text{Coef}(\text{gene}_j)$, where Expr gene_j and Coef gene_j represent prognostic gene expression levels and prognostic gene coefficients, respectively.

Then, scores indicating risk were computed for all LIHC specimens, and the median risk score was determined to stratify the samples in the TCGA-LIHC. Subsequently, risk curve plots and survival status plots were drawn to display the distribution of samples in two risk cohorts. Then, the survminer package (v 0.4.9) was used for K-M to ascertain the distinctions in survival status between the two cohorts ($p < 0.05$). After that, survivalROC package (v 0.4) was utilized to generate the receiver operating characteristic (ROC) curves to assess 1, 3, and 5 year survival probabilities. The external validation cohort GSE14520 was used to validate the risk model.

Independent prognostic analysis and nomogram construction

Subsequently, an independent prognostic analysis was conducted by integrating risk score and clinical characteristics (stage (stage I/II, stage III/IV), age (≤ 60 , > 60), gender, stage T (T1/T2, T3/T4), stage N (N0, N1), stage M (M0, M1)) of tumor samples in TCGA-HCC, Wilcoxon test was done by stats package (v 3.6.2)³³ for samples with two or fewer clinical characteristics and the risk score. For samples with three or more clinical characteristics and risk score, Kruskal-Wallis test was conducted using the Kruskal.test function. The data lacking clinical characteristics were deleted. This step was aimed to examine the distribution differences in risk scores among LIHC patients with survival information who had different clinical characteristics ($p < 0.05$).

Subsequently, based on TCGA-HCC, Cox regression analysis ($p < 0.05$) and PH assumption test ($p > 0.05$) were employed to integrate risk score and clinical characteristics, thereby identifying independent prognostic factors associated with LIHC.

After that, a nomogram was built using the rms package (v 6.5-1)³⁴ based on the prognostic genes. Calibration plot and decision curve analysis (DCA) curves were generated using rms package.

Gene set enrichment analysis (GSEA)

Subsequently, relevant signaling pathways and bioinformatics of LIHC patients with survival information in two risk cohorts were explored. The reference gene set was c2.cp.kegg.v2023.1.Hs.symbols.gmt from MSigDB (<https://www.gsea-msigdb.org/gsea/msigdb/>). In all samples of the TCGA-LIHC, firstly, DEGs between two risk cohorts were identified by DESeq2 package. Then, reliant on these DEGs, cor function was adapted for calculating the Spearman correlation coefficient, using the correlation coefficient as the sorting standard. Subsequently, GSEA was performed by clusterProfiler package ($p < 0.05$, false discovery rate (FDR) < 0.25 , |normalized enrichment score (NES)| > 1). GSEA results were sorted in descending order based on the NES values and the top 5 pathways were selected for visualization.

Analyses of immune microenvironment

The ssGSEA algorithm was intended for determining the infiltration of 28 immune cell types³⁵ between two risk cohorts in the TCGA-LIHC (excluding samples with $p > 0.05$). Differential immune cells obtained by comparing 28 immune cell infiltrations ($p < 0.05$). Subsequently, the cor function was designated to analyze the correlations between the differential immune cells, as well as between prognostic genes, risk score and these immune cells (|cor| > 0.3 and $p < 0.05$).

Drug sensitivity analysis

The relevant data on 138 standard chemotherapeutic drugs were collected to review the differences in responses between two risk cohorts by querying cancer drug sensitivity genomics (GDSC, <https://www.cancerrxgene.org>) database. Within TCGA-LIHC, pRRophetic package (v 0.5) was utilized to estimate the 50% inhibitory concentration (IC_{50}) values for the drugs, and Wilcoxon test was applied to assess the differences in drug IC_{50} between two risk cohorts ($p < 0.05$). Subsequently, the top 10 drugs with the most significant differences in two risk cohorts were selected for presentation.

RNA extraction and reverse transcription-quantitative PCR (RT-qPCR)

To confirm the reliability of the identified prognostic genes, RT-qPCR was conducted using clinical specimens from individuals with LIHC and those from healthy controls. A sum of 5 tissue samples from LIHC patients with verified diagnoses, along with an equal number of 5 samples from the control group, were gathered from the First Hospital of Lanzhou University. All participants had provided their written informed consent. Medical Ethics Committee of the First Hospital of Lanzhou University granted approval for this study (LDYYLL2024-759). Then, RNA from each sample was extracted with 1 ml TRIzol reagent and 300 μ l chloroform, and its concentration was quantified with NanoPhotometer N50. The cDNA was reverse transcribed using the SweScript First Strand cDNA Synthesis Kit (Servicebio, Wuhan, China). RT-qPCR amplification was accomplished by the CFX96 Real-Time Fluorescence Quantitative PCR Instrument (Bio-Rad, California, USA) for a total of 40 cycles. One cycle consisted of 1 min of pre-denaturation at 95 °C, denaturation at 95 °C for 20 s, annealing at 55 °C for 20 s and extension at 72 °C for 30 s. Finally, the amplification curve, melting curve, and C_q value were analyzed. The relative expression levels were determined by $2^{-\Delta\Delta CT}$ method and statistical analysis and visualization were conducted using Graphpad Prism 5 (v 8.0)³⁶. Within the scope of this research, GAPDH served as a housekeeping gene to validate the precision of our findings. Details regarding the RT-qPCR reaction mixture, the sequences of the primers, and the specific conditions for amplification were provided in supplementary Tables 1, 2, and 3, respectively.

Statistical analysis

Statistical analyses were conducted in R (v 4.3.2), with Wilcoxon test engaged to differentiate cohort pairs and $p < 0.05$ indicating significance.

Results

Recognition DEGs and key module genes

Within TCGA-HCC, 8,945 DEGs were identified (7,011 genes up and 1,934 genes down) ($p_{adj} < 0.05$) (Fig. 1a and b). Subsequently, a gene co-expression network was established based on NETs-RGs through WGCNA. Initially, we scored NETs-RGs in both tumor and normal samples, and found a significant distinction in NETs-RGs scores between the two cohorts ($p = 0.024$) (Fig. 1c). Then, based on the median NRGs-RGs score, high and low scoring cohorts were divided, K-M curve showed a significant survival difference between two scoring cohorts ($p = 0.00049$) (Fig. 1d). Next, hierarchical clustering analysis was performed on all samples and identified no obvious outliers (Fig. 1e). Subsequently, the optimal soft-thresholding power was determined to be $\beta = 10$ ($R^2 > 0.85$) (Fig. 1f). Then, a hierarchical clustering dendrogram was constructed, dividing the genes into 11 co-expression modules (Fig. 1g). Ultimately, MEbrown module ($cor = -0.78$, $p = 7e-77$) was selected as the key module (Fig. 1h), and the 1,870 genes within MEbrown module were designated as key module genes.

Recognition and functional annotation of candidate genes

By intersecting DEGs, IRGs and key module genes, 78 candidate genes were obtained (Fig. 2a, supplementary Table 4). The overlapping situations of these genes with NET-RGs were examined, identified 5 overlapping genes including MMP9, FPR1, IL1B, IL6 and FPR2 (Supplementary Fig. 1). This could help to highlight the potential role of NETs in hepatocellular carcinoma. GO analysis found that these candidate genes enriched in 316 terms, including 31 molecular functions (MF), 7 cellular components (CC) and 278 biological processes (BP), with the top 10 enriched terms comprising immunoglobulin production and leukocyte mediated immunity ($p_{adj} < 0.05$) (Fig. 2b). Additionally, KEGG enrichment identified 22 signaling pathways, including cytokine-cytokine receptor interaction and cytokine receptor ($p_{adj} < 0.05$) (Fig. 2c). Subsequent PPI results showed that 30 genes had no interaction relationships, while CETP, PTGER2, GBP2, and UTS2 each had only one interaction (interaction score > 0.4) (Fig. 2d). After removing these 30 genes without interaction relationships, 48 candidate genes were used for further research (supplementary Table 5).

Prognostic model development and evaluation

Based on all tumor samples with survival information in TCGA-HCC, five candidate prognostic genes were determined through univariate Cox regression analysis including HMOX1 (HR = 1.22, 95% CI: 1.07–1.40, $p = 0.003$), MMP9 (HR = 1.14, 95% CI: 1.03–1.26, $p = 0.011$), TNFRSF4 (HR = 1.33, 95% CI: 1.06–1.66, $p = 0.01$), MMP12 (HR = 1.16, 95% CI: 1.02–1.32, $p = 0.02$), FLT3 (HR = 0.23, 95% CI: 0.07–0.81, $p = 0.02$), among which only FLT3 was a protective gene (HR < 1) (Fig. 3a). Univariate Cox regression analysis was conducted to evaluate the association strength and statistical significance between each gene and the prognosis of HCC patients by calculating the HR values, their 95% CIs, and p-values. The p-values of these five genes were all less than 0.05, indicating that there were statistically significant associations between them and the survival of HCC patients, and the null hypothesis of no association between gene expression and survival outcome was rejected. Meanwhile, the HR values of HMOX1, MMP9, TNFRSF4, and MMP12 were greater than 1, while the HR value of FLT3 was less than 1, and the 95% CIs of each did not contain 1, which further supported the correlations between these genes and the prognosis of HCC. This demonstrated that obtaining these five genes through

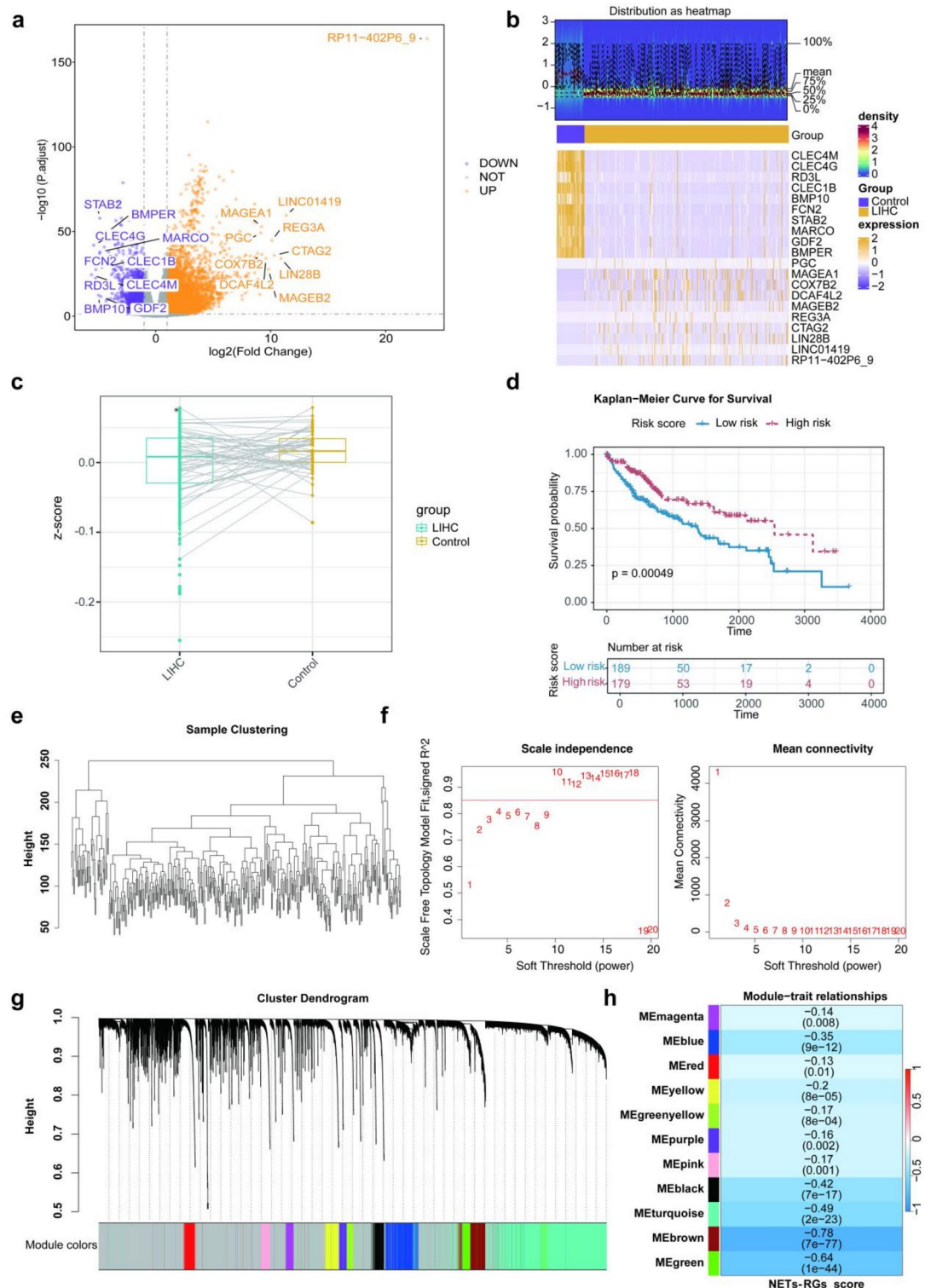


Fig. 1. Screening for DEGs. **(a)** Volcano plot of DEGs in TCGA-HCC. **(b)** Heatmap of DEGs in TCGA-HCC. The numerical range was from -1 to 3, representing values related to gene expression levels. The legend on the right side showed that colors corresponded to expression densities, with red indicating high expression density and blue indicating low expression density. The black lines represented different quantiles, such as 0%, 25%, 50%, 75%, and 100%, and the data distribution between tumor and normal samples was presented. **(c)** NETs-RGs scores between tumor and normal samples. **(d)** The survival probability of the two risk groups. Blue represents patients in low risk group and red represents patients in high risk group (p -value = 0.00049) LIHC = 374, control = 50, NETs-RGs = 87. **(e)** The hierarchical clustering analysis among all samples. **(f)** Determination of the soft thresholding power. The y-axis of the left panel represents the scale-free fit index and the y-axis of the right panel represents the mean connectivity. The x-axis represents power value. **(g)** Dendrogram of differentially expressed genes clustered. The colors represent the identified gene modules. **(h)** Correlations of gene modules with NETs-RGs scores.

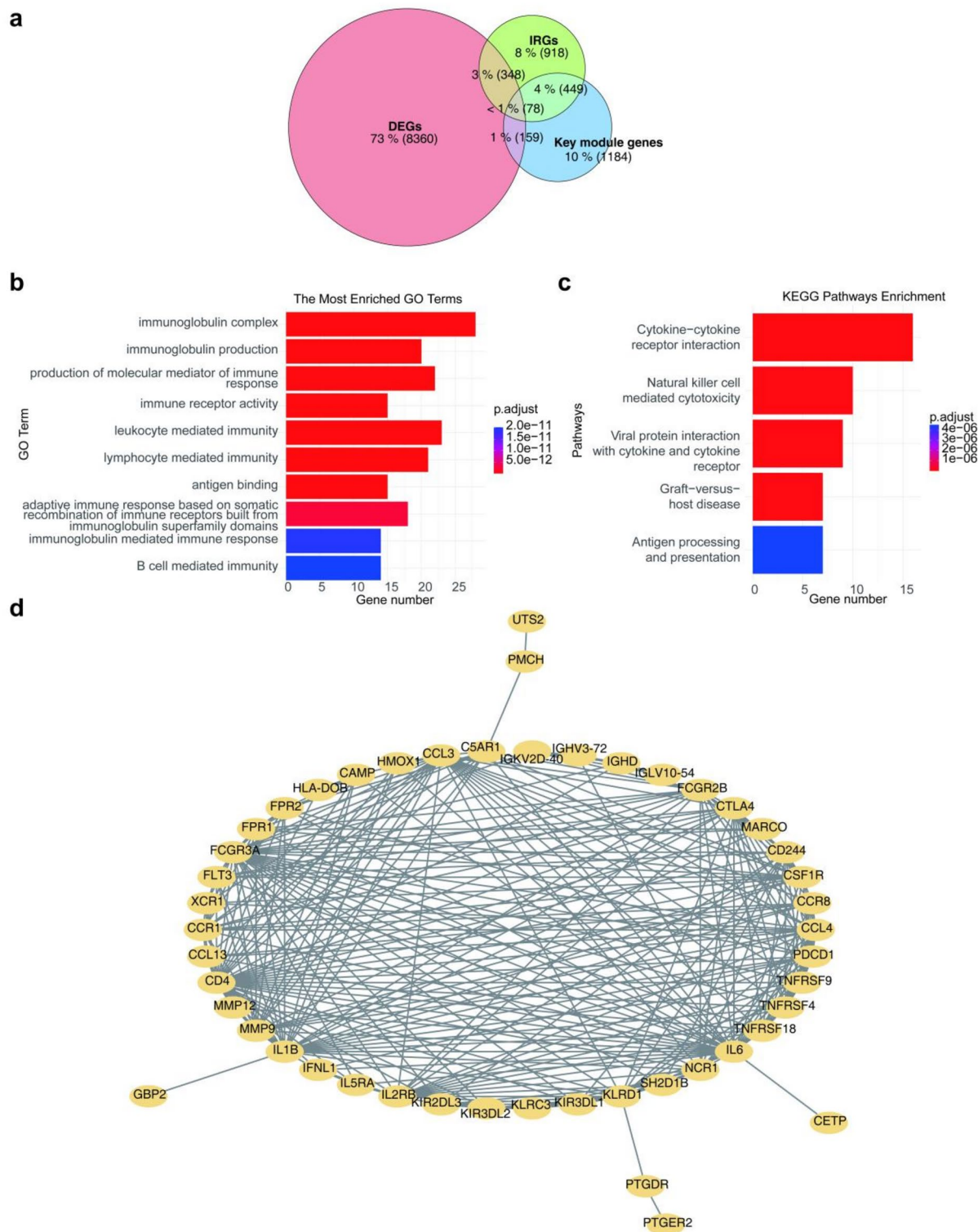


Fig. 2. Acquisition and functional enrichment analysis of candidate genes. **(a)** Venn diagrams of candidate genes, DEGs = 8945, IRGs = 1793, and key module genes = 1870. **(b)** The GO outcomes are displayed with a histogram. **(c)** A histogram was constructed to illustrate the KEGG outcomes. GO, Gene Ontology; KEGG, Kyoto Encyclopedia of Genes and Genomes; BP, biological process; CC, cellular component; MF, molecular function. **(d)** Screening 48 candidate genes by PPI network.

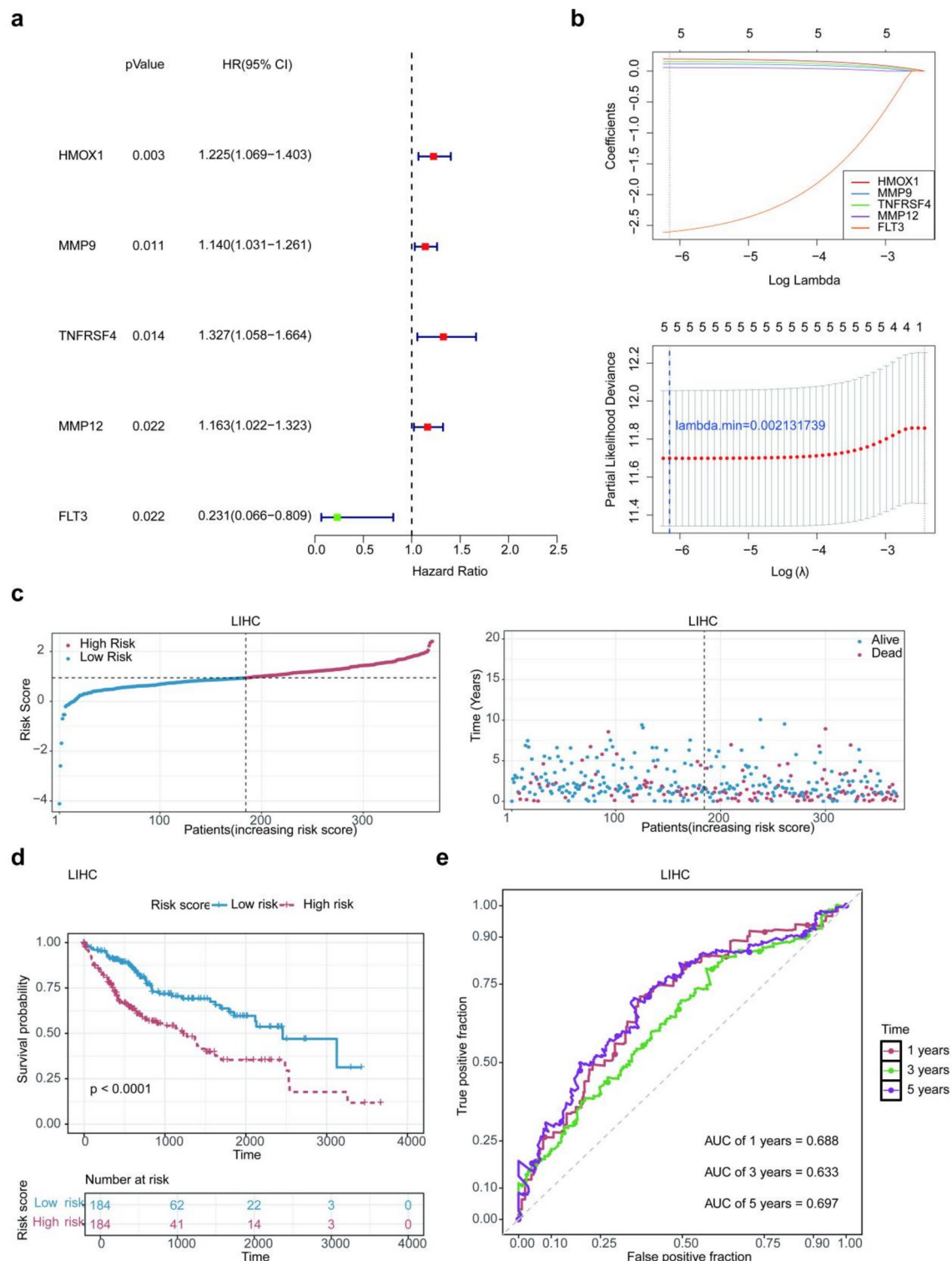


Fig. 3. Construction of a prognostic model in TCGA-HCC. **(a)** Univariate Cox regression analysis in TCGA-HCC. **(b)** Coefficient curve. Different colors represent different genes. No zero values were selected as a penalty coefficient (Left). The minimum lambda of the lasso model was selected via 10 folds of cross-validation. Lambda was determined when the partial likelihood deviance was smallest (Right). **(c)** The risk score of the different risk groups. **(d)** The survival probability of the different risk groups. Blue represents high-risk patients and red represents low-risk. The patients were divided according to their median risk score. **(e)** Prognostic genes in the TCGA-HCC dataset were analyzed using ROC curves.

univariate Cox regression analysis was reasonable and statistically grounded. Subsequently, the PH assumption test was conducted for these five genes, and all five genes passed the test (supplementary Table 6). Then, LASSO analysis was performed on these five candidate prognostic genes, and it was found that when $\lambda = 0.002$, the penalty values for all five candidate prognostic genes were not zero (Fig. 3b). The Bootstrap results showed that the mean value of the coefficient of *HMOX1* was 0.2009, with the hazard ratio (HR) approximately equal to 1.22 ($\exp(0.2009) \approx 1.22$), and the mean value of the coefficient of *FLT3* was -1.5377 , with the HR approximately equal to 0.215 ($\exp(-1.5377) \approx 0.215$). The small standard deviations indicated that the coefficient estimations were stable. For example, the maximum standard deviation (SD) of *TNFRSF4* was 0.124, which showed that the stability of its coefficient estimation was relatively low. The minimum SD of *MMP9* was 0.05, suggesting that its coefficient estimation was relatively stable. The 95% confidence intervals (CIs) of all genes did not contain 0, which was consistent with the result of the univariate Cox regression analysis with $p < 0.05$, verifying the significance (supplementary Table 7). Therefore, *HMOX1*, *MMP9*, *TNFRSF4*, *MMP12*, and *FLT3* were retained as prognostic genes for further research.

Next, a risk model was established using the expression levels of these five prognostic genes and coefficients derived from LASSO analysis to determine the risk scores for LIHC patients: Risk Score = $0.20 \times HMOX1 + 0.12 \times MMP9 + 0.154 \times TNFRSF4 + 0.06 \times MMP12 - 2.60 \times FLT3$. Then, the risk scores for tumor samples in TCGA-HCC (0.94) and GSE14520 (-6.83) were calculated, and patients were categorized into two distinct risk cohorts based on the median risk score. The distribution pattern of risk scores and the associated survival outcomes were graphed based on the patients' risk scores in ascending order, demonstrating that a higher risk score was significantly associated with a higher mortality rate (Fig. 3c and Supplementary Fig. 2a). K-M analysis revealed that the high-risk group had a markedly lower survival rate across both datasets ($p < 0.05$) (Fig. 3d and Supplementary Fig. 2b). In the TCGA-HCC, ROC analysis further confirmed its accuracy in predicting the survival rates at 1 (0.69), 3 (0.63) and 5 years (0.70) (for GSE14520, the values were 0.68, 0.68 and 0.63) (Fig. 3e and Supplementary Fig. 2c).

Nomogram construction and clinical characteristic analysis

Cox analysis and PH assumption test indicated that risk score emerged as the sole independent predictor of prognosis for LIHC ($p < 0.05$) (Fig. 4a and b and supplementary Table 8). Then, a nomogram was built via prognostic genes (Fig. 4c). The calibration plots exhibited that the nomogram's predictions for 1, 3, and 5 year survival probabilities closely matched the actual outcomes, aligning well with the reference line, indicating a high level of predictive accuracy (Fig. 4d). Following that, the results from DCA portrayed a net benefit above zero for the nomogram, signifying its effective construction (Fig. 4e). Clinical characteristic analysis revealed significant differences in risk scores among stages and T stages ($p < 0.05$) (Fig. 4f). The risk score was higher in the T3/T3 group than in the T1/T2 group, and it was higher in the stage III/IV group than in the stage I/II group. This indicated that the risk score was closely associated with the tumor stage of LIHC. A higher risk score might have predicted a more advanced tumor stage. It was suggested that clinicians could incorporate the risk score into the disease assessment system for LIHC patients to assist in judging the disease progression degree of patients. This would enable timely adjustment of treatment regimens and adoption of more targeted intervention measures to improve patient prognosis.

Enrichment, immune landscape and drug sensitivity in two risk cohorts

The DEGs in two risk cohorts were primarily enriched in retinol metabolism and drug metabolism cytochrome p450 (Fig. 5a). The heatmap of 28 different immune cells showed in the Supplementary Fig. 3 between two risk cohorts, with statistical difference in 16 immune cells, including regulatory T cells and MDSCs (Fig. 5b). Subsequently, Spearman's correlation analysis indicated that regulatory T cells were statistically positively correlated with MDSCs ($\text{cor} = 0.89$, $p = 9.13 \times 10^{-126}$) (Fig. 5c and supplementary Table 9). The correlation analysis between differential immune cells and prognostic genes showed that MDSCs had notable link to *HMOX1* ($\text{cor} = 0.54$), *MMP9* ($\text{cor} = 0.62$), *TNFRSF4* ($\text{cor} = 0.48$), *MMP12* ($\text{cor} = 0.43$), and *FLT3* ($\text{cor} = 0.43$) (Fig. 5d and supplementary Table 10).

In drug sensitivity analysis, 74 drugs showed substantial discrepancies between the two risk cohorts ($p < 0.05$). Axitinib and AS601245 had higher IC_{50} values in the high-risk cohort, while ABT.888 and A.443,654 had lower IC_{50} values (Fig. 5e).

Experimental validation of prognostic genes

As shown in Fig. 6, the results of RT-qPCR analysis indicated that the expression levels of *HMOX1* ($p < 0.01$) and *FLT3* ($p < 0.05$) in LIHC tissues were significantly decreased compared to the control, while the expression of *MMP9* ($p < 0.05$) and *TNFRSF4* ($p < 0.0001$) were the opposite. Although the expression of *MMP12* ($p > 0.05$) was elevated in LIHC, there was no significant difference compared to the control group. In LIHC tissues, the expression levels of *HMOX1* and *FLT3* were significantly decreased compared to the control group. The significant changes in gene expression implied a close association with the disease state. When LIHC occurred in the body, the down-regulation of these two genes might have affected a series of key physiological processes within the cells. The expression of *MMP9* and *TNFRSF4* in LIHC tissues showed an opposite trend to that of *HMOX1* and *FLT3*, and was significantly higher than that in the control group. The significantly up-regulated expression of these two genes in LIHC tissues reflected their active roles in the process of tumorigenesis and development. Therefore, they could be used as potential biomarkers for monitoring the progression of LIHC or evaluating the prognosis of patients. The expression of *MMP12* was elevated in LIHC tissues, but there was no significant difference compared to the control group. However, its expression trend still indicated a certain connection with the LIHC state. Although the current results did not reach statistical significance, under a

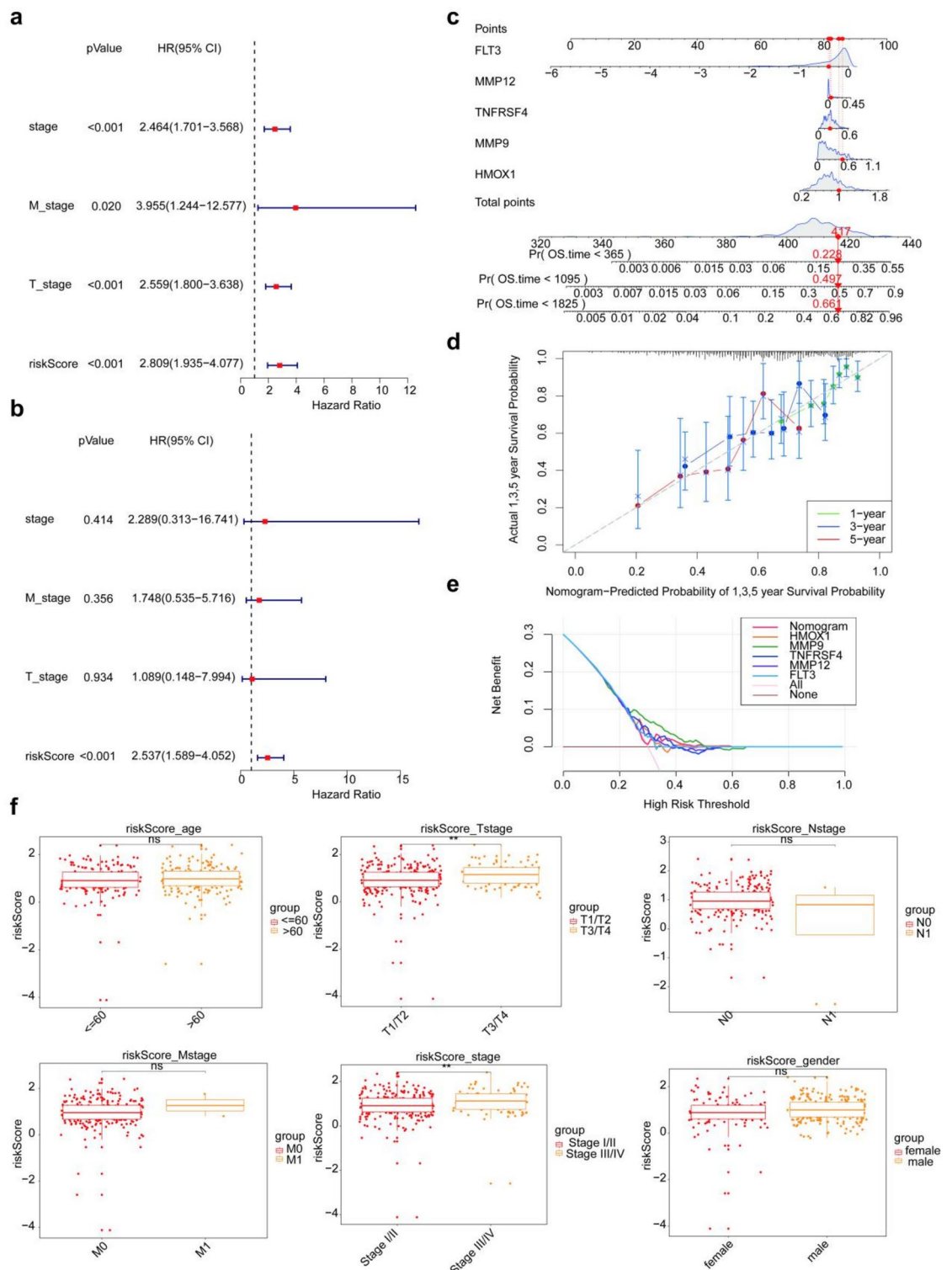


Fig. 4. Construction of nomogram and analysis of clinical characteristic with riskScore. **(a)** Univariate Cox regression and multivariate Cox regression **(b)** analyses of independent predictor of prognosis for LIHC. **(c)** Nomogram was constructed based on the expression of prognostic genes. **(d)** Calibration curves of nomogram for predicting OS at 1-year, 3-year and 5-year in the TCGA-HCC dataset. **(e)** DCA curves were constructed based on prognostic genes. **(f)** Box plots of clinical characteristic (age, T_stage, N_stage, M_stage, stage, and gender) between subgroup in the TCGA-HCC cohort. * $p < 0.05$; ** $p < 0.01$; *** $p < 0.001$; **** $p < 0.0001$; ns $p > 0.05$.

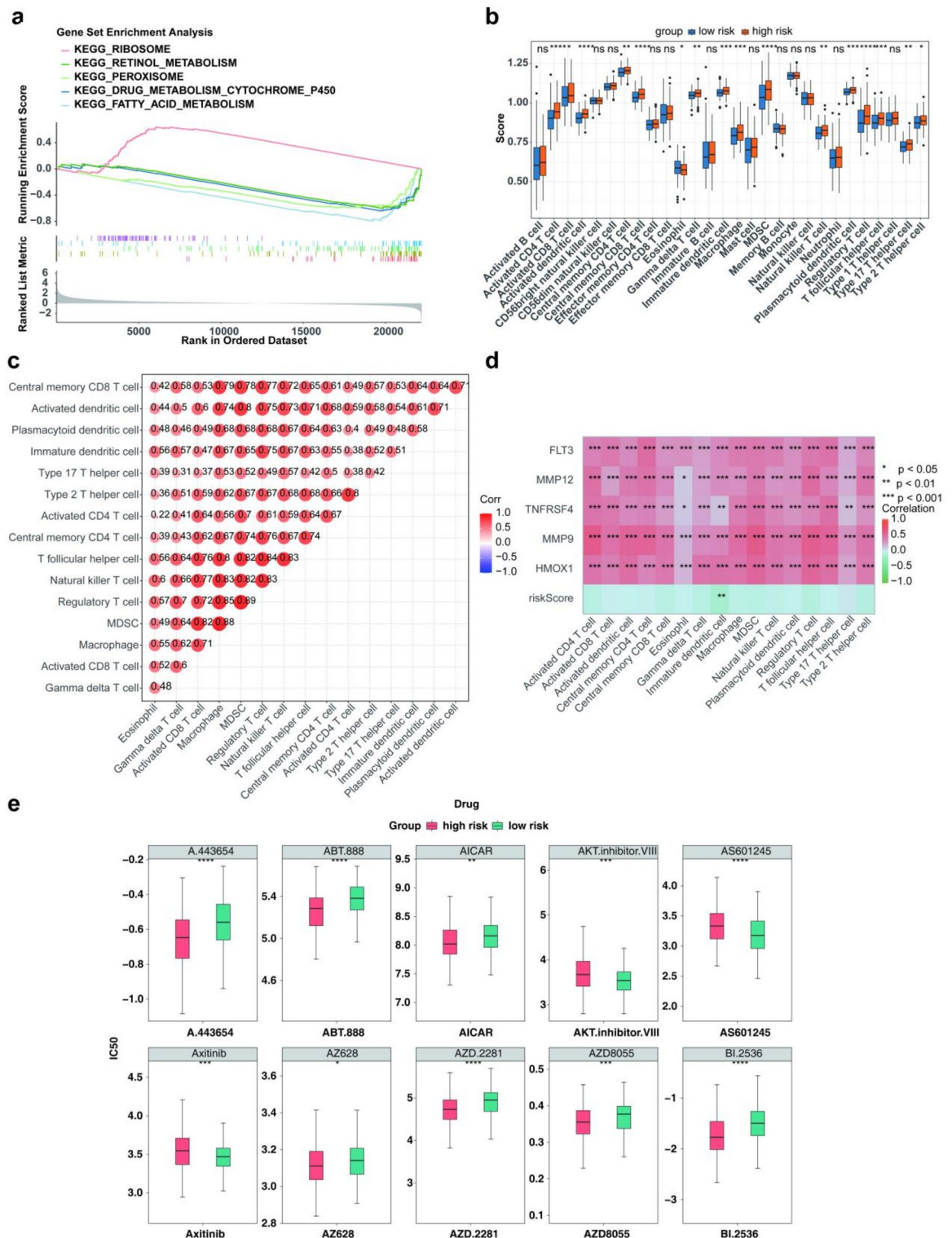


Fig. 5. Analysis of GSEA, immune microenvironment, and drug sensitivity. **(a)** Significantly enriched pathways in the KEGG gene sets between the two risk groups in TCGA-HCC cohort. **(b)** Box plot of the difference in immune cell content between two risk groups. **(c)** Correlations between infiltrating immune cells. Red and blue colors indicate positive and negative correlations, color intensity represents the degree of correlation. **(d)** Correlations between infiltrating immune cells and prognostic genes. **(e)** The differences of sensitivity of patients between two risk groups. Lower IC50 is equal to better sensitivity. * $p < 0.05$; ** $p < 0.01$; *** $p < 0.001$; **** $p < 0.0001$; ns $p > 0.05$.

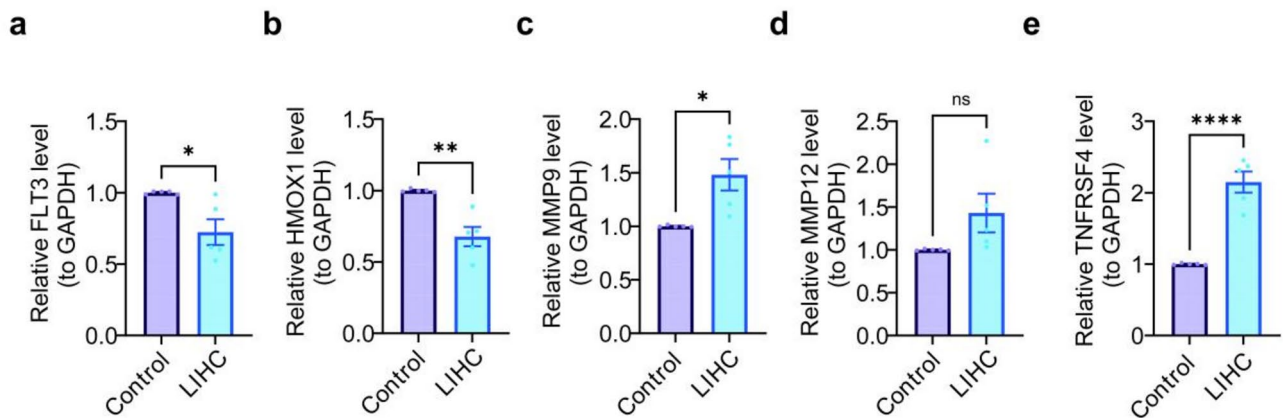


Fig. 6. Relative mRNA expression of the prognostic genes was analyzed by qRT-PCR. * $p < 0.05$; ** $p < 0.01$; *** $p < 0.001$; **** $p < 0.0001$; ns $p > 0.05$, $n = 6$.

larger sample size or different research conditions, the changes in its expression might provide more information related to LIHC, and it still had the potential to be used as an auxiliary biomarker.

Discussion

HCC is one of the most common cancers worldwide and represents a major challenge for healthcare worldwide³⁷. Hundreds of thousands of people die from HCC globally each year, with most patients diagnosed at a late stage, missing the optimal window for treatment³⁸. Effective and reliable prognostic biomarkers are crucial for clinical treatment. Currently, new studies have emphasized that NETs facilitated immune escape from HCC³⁹. This study examined the expression levels of genes reported in the literature to be associated with NETs¹⁹ and immune in HCC and healthy samples and found that most of these genes were differentially expressed. Subsequently, a new prognostic model consisting of *HMOX1*, *FLT3*, *MMP9*, *MMP12*, *TNFRSF4* and was constructed using univariate Cox and LASSO, followed by an in-depth analysis of the immune microenvironment.

In biological research, various molecules play diverse and crucial roles in different immune cell types, having a significant impact on aspects such as cell function, disease development, and immune responses. Specifically, *HMOX1* is expressed in macrophages, where it assumes a pivotal role in intracellular oxidative stress responses and immune regulation, contributing to the maintenance of normal macrophage function⁴⁰. *FLT3* is predominantly expressed in dendritic cells, where it is closely associated with their development, maturation, and antigen - presenting functions, thus influencing the body's immune response⁴¹. Neutrophils are capable of expressing *MMP9*, which is released during inflammation and tissue repair to degrade the extracellular matrix, facilitating the migration of inflammatory cells and tissue remodeling⁴². *MMP12* is highly expressed in alveolar macrophages, where it takes part in lung inflammation and tissue repair by degrading the extracellular matrix of alveolar walls, and is related to the development of lung diseases such as chronic obstructive pulmonary disease^{43,44}. Monocytes may also express *MMP12* during their differentiation into macrophages, participating in inflammatory responses and immune regulation, and playing a part in the body's innate immune defense⁴⁵. Besides CD4 + T cells, other T - cell subsets, such as CD8 + T cells, can also express *TNFRSF4*, which is involved in T - cell activation, proliferation, and immune regulation, affecting the intensity and duration of T - cell - mediated immune responses^{46,47}. Antigen - presenting cells like macrophages and dendritic cells also express *TNFRSF4*, where it interacts with T cells during antigen presentation to regulate the balance between immune activation and immune tolerance⁴⁸.

Heme Oxygenase 1 (*HMOX1*) is a catalytic enzyme that facilitates the degradation of heme into iron, carbon monoxide and biliverdin, playing a significant role in cellular response to inflammation⁴⁹. Studies have indicated that in HCC, the tumor microenvironment is marked by a high level of oxidative stress. The up-regulation of *HMOX1* might change the activation pattern of neutrophils, thus promoting the release of NETs^{48,50}. Nevertheless, the chronic and excessive release of NETs can result in an imbalance within the inflammatory microenvironment, creating conditions that are conducive to the proliferation and metastasis of tumor cells⁵¹. This could act as a double-edged sword in the progression of HCC, and the regulatory role of *HMOX1* on NETs is one of the crucial factors affecting this balance. In our study, the results of the univariate Cox regression analysis indicated that the HR for *HMOX1* was 1.225, with a p value of 0.003. Specifically, within a 95% confidence interval of 1.069–1.403, a one - unit increase in *HMOX1* expression was significantly associated with a 22.5% increase in the risk of disease progression or death in HCC patients. Since *HMOX1* has been identified as a risk factor for HCC, it is hypothesized that *HMOX1* might be involved in the biological processes promoting the growth, invasion, or metastasis of HCC, thus playing a crucial role in the development and prognosis of HCC⁵². Park et al. found that *HMOX1* expression was not associated with patient survival or recurrence, indicating that *HMOX1* does not appear to play a role as a prognostic factor in HCC patients⁵³. Nevertheless, Zheng et al. confirmed through chromosome conformation capture experiments that Donafenib and GSK-J4 synergistically induce ferroptosis in HCC by up-regulating *HMOX1* expression, which represented a novel synergistic lethal interaction⁵⁴. Over-expression of *HMOX1* reduced the proliferation of human HBV-HCC cells and inhibited their migratory and

invasive capabilities⁵⁵. There were also suggested that *HMOX1* may be regarded as a favorable prognostic factor in HBV-HCC patients undergoing liver resection⁵⁶.

Fms-like tyrosine kinase 3 (*FLT3*) is a significant member of the class III receptor tyrosine kinase (RTK) family, playing a crucial role in the proliferation of hematopoietic cells and lymphocytes⁵⁷. Although current research regarding the direct connection between *FLT3* and NETs is scarce, considering that neutrophils are derived from hematopoietic stem cells, abnormal *FLT3* signaling might change the differentiation pathway of hematopoietic stem cells⁵⁸. Consequently, this could impact the quantity and functional status of neutrophils, thus indirectly affecting the generation of NETs. Aydin discovered that *FLT3* is pivotal in the initiation and progression of HCC. Targeting *FLT3* may represent a promising strategy for combating this tumor⁵⁹. In our study, the HR for *FLT3* was 0.231, with a p value of 0.022, suggesting that *FLT3* is a protective gene in HCC. An increase in *FLT3* expression is associated with a decreased risk of HCC. The 95% confidence interval of 0.066–0.809 further validates this finding. Thus, *FLT3* might be involved in pathways that inhibit the growth of HCC, induce apoptosis of cancer cells, or enhance the immune response against HCC cells⁶⁰. Lai found that novel *FLT3* / AURK multikinase inhibitors were effective against sorafenib-resistant HCC⁵⁷. Further studies have shown that sorafenib can slow down the progression of tumors in HCC patients who exhibit high levels of *FLT3* expression⁶¹. In this study, the expression of *HMOX1* and *FLT3* in the HCC group was notably lower compared to healthy groups, signifying its positive factors in the prognosis of HCC.

Matrix metalloproteinase-9 (MMP9) is a crucial mediator of tumor initiation and progression⁶². In our study, univariate Cox regression analysis demonstrated that the HR for *MMP9* was 1.140, with a p value of 0.011. This finding suggests that *MMP9* serves as a risk factor for HCC. An elevated level of *MMP9* expression is correlated with an increased risk of HCC and might facilitate the biological processes related to its growth, invasion, or metastasis⁶³. In HCC, *MMP9* expression is significantly elevated in the gain of function (GOF) CTNNB1 mutations (CTNNB1^{GOF}), so CTNNB1^{GOF} mutations promoted the formation of an inhibitory tumor micro-environment by triggering *MMP9* secretion⁶⁴. In HBV-infected HCC patients, Chen et al. found that HBV stimulated peripheral blood mononuclear cells (PBMCs) and macrophages to express MMP-9. More interestingly, MMP9 in turn promotes HBV replication by inhibiting the effects of IFN- α ⁶⁵. Meanwhile, previous studies have suggested that VEGFA signal could activate tumor-associated macrophages (TAM) _ SPP1-derived *MMP9* to promote the invasion and metastasis of HCC, which may provide new insights into the clinical treatment of HCC patients⁶⁶. Moreover, targeted drug studies have revealed that indirubin effectively combats metastatic HBV-positive HCC by inhibiting the activity of *MMP9*⁶⁷.

Matrix metalloproteinase-12 (*MMP12*), also known as macrophage metalloelase, was first identified in human alveolar macrophages⁶⁸. Univariate Cox regression analysis disclosed that the HR for *MMP12* was 1.163, with a p - value of 0.02. This finding implies that *MMP12* is a risk factor for HCC. An elevated expression of *MMP12* is associated with an increased risk of HCC and may be implicated in biological processes promoting the growth, invasion, or metastasis of HCC⁶⁹. Many studies have shown that the over-expression of *MMP12* is associated with the poor prognosis of HCC, which may be an important factor affecting the efficacy of TACE^{70–72}. Furthermore, He et al. found that *MMP12* expression was associated with tumor FOXP3 regulatory T cell infiltration and poor prognosis in HCC⁶⁸. However, some studies have proposed that blood MMP-12 has good sensitivity and higher accuracy but poor specificity in the diagnosis of HCC⁶⁹. *MMP9* and *MMP12* might degrade the extracellular matrix around NETs, thus influencing the structural stability and distribution of NETs⁶⁹. In HCC, the heightened levels of *MMP9* and *MMP12* secreted by tumor cells not only facilitate tumor cell invasion and metastasis by breaking down the basement membrane but also potentially modify the existence of NETs in the tumor microenvironment⁷³. During the invasion and metastasis process in HCC, the interaction among *MMP9*, *MMP12*, and NETs seems to be especially intricate and significant⁷⁴.

Tumor Necrosis Factor Receptor Superfamily Member 4 (*TNFRSF4*), named OX40, is an important costimulatory molecule for T cell proliferation and survival, plays a key role in regulating the immune response, cell survival and the inflammatory response⁷⁵. Research findings indicate that the activation of the *TNFRSF4* signaling pathway can impact neutrophil function, thereby influencing the generation of NETs⁷⁶. In HCC, tumor cells may disrupt the normal functioning of neutrophils and modulate the release and activity of NETs by regulating the *TNFRSF4* signaling pathway⁷⁷. Univariate Cox regression analysis revealed that the HR for *TNFRSF4* was 1.327, with a p-value of 0.014. This indicates that *TNFRSF4* is a risk factor for HCC. Elevated expression of *TNFRSF4* is associated with an increased risk of HCC and may be involved in biological processes that promote the growth, invasion, or metastasis of HCC⁷⁷. Interestingly, Yan et al. found that the expression of *TNFRSF4* in HCC was significantly higher than in normal tissues, which was identified as a risk factor for overall survival in male patients⁷⁷. Notably, Wang et al. found that the over-expression of *TNFRSF4* affected the immune cell infiltration in HCC⁷⁶. Studies have proposed the combined intratumoral administration of CpG and anti-*TNFRSF4* antibodies as a promising immunotherapy approach for HCC⁷⁸. In this study, we also observed that the expression of *TNFRSF4* and *MMP9* in the HCC group was notably higher compared to the healthy group, which confirmed that their high expression was associated with poor prognosis.

Furthermore, the enrichment analysis revealed that those DEGs in two risk groups were primarily enriched in 'drug metabolism cytochrome p450' signaling pathway. Cytochrome P450, a group of enzymes predominantly expressed in the liver, plays a pivotal role in numerous biochemical processes⁷⁹. One study suggested that cytochrome P450 2E1 plays a dynamic role in the pathogenesis of HCC, which could serve as a potential therapeutic target for liver carcinogenesis⁸⁰. In this study, we hypothesized that the expression of these five biomarkers affects the progression of HCC by participating in 'drug metabolism cytochrome p450' signaling pathway. Additionally, we found that Axitinib had higher IC50 values in the high-risk cohort, which confirmed that the combination of Axitinib proposed by Yang et al. was well tolerated in the treatment of advanced HCC⁸¹.

The role of the tumor TME was receiving heightened attention due to its substantial impact on clinical outcomes and therapeutic responses⁸². In this study, 28 different types of immune cells were specifically selected for analysis.

This is because these cells represent multiple key aspects of the tumor immune response. For example, Tregs, as crucial regulators of the immune response, can inhibit the activity of effector T cells, thereby impeding the body's immune surveillance and killing of tumor cells^{83,84}. MDSCs also play a central role in immunosuppression. They can inhibit the functions of immune cells through various mechanisms, creating conditions for the immune escape of tumor cells⁸⁵. We found that MDSC (myeloid derived suppressor cell) had notable link to *HMOX1*, *MMP9*, *TNFRSF4*, *MMP12* and *FLT3*. Higher infiltration of MDSCs in HCC compared to controls⁸⁶. Li et al. proposed that MDSC-targeted therapy may be the best choice for HCC patients with higher neutrophil counts⁸⁷. In detail, MDSCs exhibit a positive correlation with *HMOX1* ($\text{cor} = 0.54$). This correlation indicates that MDSCs may up-regulate the expression level of *HMOX1*, assisting HCC cells in withstanding oxidative stress, thereby enhancing their survival ability and promoting tumor progression⁸⁸. *MMP9* has the function of degrading the extracellular matrix, creating conditions for the migration and invasion of HCC cells^{89,90}. Meanwhile, there is a strong correlation between MDSCs and *MMP9* ($\text{cor} = 0.62$), suggesting that MDSCs may enhance the invasion and metastasis ability of HCC cells by promoting the expression of *MMP9*, exerting a crucial impact on the malignant development process of HCC⁹¹. *TNFRSF4* is involved in the regulation of immune cell activation and proliferation, and MDSCs are associated with it ($\text{cor} = 0.48$). MDSCs may inhibit the functions of immune cells by interfering with the *TNFRSF4* related immune-regulatory signaling pathways, thus helping HCC cells achieve immune escape⁹². *MMP12* is also associated with MDSCs ($\text{cor} = 0.43$). Its function is similar to that of *MMP9* and can promote the metastasis of HCC cells by degrading the extracellular matrix⁹³. *FLT3* plays an important role in the proliferation and differentiation of hematopoietic stem cells. In HCC, when *FLT3* is abnormally activated, it can promote the growth and survival of tumor cells⁹⁴. The association between MDSCs and *FLT3* ($\text{cor} = 0.43$) implies that MDSCs may be involved in regulating the proliferation and survival signaling pathways of HCC cells⁹⁵. Therefore, we believed that these five biomarkers may influence the occurrence of HCC by regulating the expression of MDSC to regulate the immune microenvironment of HCC. This finding further supports our belief that *HMOX1*, *MMP9*, *TNFRSF4*, *MMP12* and *FLT3* have potential as biomarkers in HCC and we remain keenly interested in exploring their specific molecular mechanisms.

Drug-sensitivity analysis showed that 74 drugs exhibited significant differences between the two risk groups ($p < 0.05$). The IC_{50} value, a key indicator of drug potency, varied significantly for specific drugs across different risk cohorts. Specifically, Axitinib and AS601245 had higher IC_{50} values in the high-risk group, indicating that patients in the high-risk group require higher concentrations of these two drugs to achieve 50% cell-growth inhibition⁹⁶. This suggests that tumor cells in the high-risk group may have stronger drug-resistance mechanisms, such as enhanced drug efflux pump activity or altered drug targets⁹⁷. For these patients, conventional doses of Axitinib and AS601245 may not be effective. Clinicians may need to consider increasing the drug doses, which may lead to more severe side effects, or explore combination-drug regimens to enhance the efficacy of these two drugs using other agents⁹⁸. In contrast, ABT.888 and A.443,654 had lower IC_{50} values in the high-risk cohort, indicating that the high-risk group is more sensitive to these two drugs. ABT.888, as a poly (ADP-ribose) polymerase (PARP) inhibitor, can specifically act on tumor cells with DNA damage repair defects⁹⁹. It is speculated that tumor cells in the high-risk group may have abnormal DNA repair pathways, making ABT.888 and A.443,654 more effective, so low-dose administration can be used to enhance efficacy and reduce side effects. Based on the above findings, targeted therapy has broad prospects. For example, high-risk patients who are resistant to Axitinib but sensitive to ABT.888 can try ABT.888 targeted therapy. Similarly, the low-risk cohort can also select drugs according to IC_{50} values and tumor characteristics. Looking ahead, clinical research should conduct large-scale trials for different patient subgroups, use techniques such as whole-genome sequencing to clarify the associations between drug sensitivity and genetic and clinical characteristics, establish prediction models, and study the dynamic changes during treatment to optimize treatment strategies and improve the clinical outcomes of cancer patients.

Currently, the samples used in this study were sourced from bulk RNA-sequencing samples in public databases, and it may not be possible to precisely distinguish the signals of each cell type. In follow-up research, single-cell RNA sequencing or other cell-isolation techniques will be employed to further validate which cell types these signals specifically originate from. In addition, the small sample size of RT-qPCR may lead to large result deviations and insufficient representativeness, making it difficult to reflect the overall real situation. Clinical samples will be increased for research in the future. Moreover, research on 28 types of immune cells also lacks experimental support. Techniques such as flow cytometry and immunohistochemical experiments should be used to verify their characteristics and functions. The role network of *HMOX1*, *MMP9*, *TNFRSF4*, *MMP12* and *FLT3* in the progression of HCC requires further constructed in cell experiments and animal models for functional exploration. In future research, specific markers can be employed to sort neutrophils, and cell-lines can be utilized to investigate the expression patterns of *TNFRSF4* in different immune cells. Meanwhile, experiments should be conducted to verify the types of immune cells. Moreover, the dataset used in this study lacks treatment history and comorbidity data. Future research should collect more of such data and carry out in-depth investigations into treatment history and comorbidities, so as to provide more evidence for personalized treatment. We plan to further explore these mechanisms through molecular approaches in the future.

Conclusion

The risk model constructed by the signature composed of *HMOX1*, *MMP9*, *TNFRSF4*, *MMP12* and *FLT3* can predict the prognosis of HCC patients, and these biomarkers were related to tumor immunity. This study provides a novel direction, theoretical foundation and potential target therapy for HCC. Our findings confirm the up-regulation of *MMP9*, *TNFRSF4* and down-regulation of *HMOX1*, *FLT3* in HCC patients, which presents a fresh perspective for the treatment of HCC.

Data availability

The datasets analysed during the current study are available in the GEO database (<https://www.ncbi.nlm.nih.gov/geo/>) and TCGA database (<https://portal.gdc.cancer.gov/>).

Received: 22 January 2025; Accepted: 5 May 2025

Published online: 03 June 2025

References

- Brown, Z. J. et al. Management of hepatocellular carcinoma: A review. *JAMA Surg.* **158**, 410–420. <https://doi.org/10.1001/jamasurg.2022.7989> (2023).
- Gilles, H., Garbutt, T. & Landrum, J. Hepatocellular carcinoma. *Crit. Care Nurs. Clin. North. Am.* **34**, 289–301. <https://doi.org/10.1016/j.cnc.2022.04.004> (2022).
- Chan, Y. T. et al. Biomarkers for diagnosis and therapeutic options in hepatocellular carcinoma. *Mol. Cancer.* **23**, 189. <https://doi.org/10.1186/s12943-024-02101-z> (2024).
- Nevola, R. et al. Predictors of early and late hepatocellular carcinoma recurrence. *World J. Gastroenterol.* **29**, 1243–1260. <https://doi.org/10.3748/wjg.v29.i8.1243> (2023).
- Karachaliou, G. S., Dimitrakakis, N. & Moris, D. P. Downstaging strategies for unresectable hepatocellular carcinoma. *World J. Gastroenterol.* **30**, 2731–2733. <https://doi.org/10.3748/wjg.v30.i20.2731> (2024).
- Piñero, F., Dirchwolf, M. & Pessoa, M. G. Biomarkers in Hepatocellular Carcinoma: Diagnosis, Prognosis and Treatment Response Assessment. *Cells* **9**. <https://doi.org/10.3390/cells9061370> (2020).
- Singal, A. G. et al. HCC surveillance improves early detection, curative treatment receipt, and survival in patients with cirrhosis: A meta-analysis. *J. Hepatol.* **77**, 128–139. <https://doi.org/10.1016/j.jhep.2022.01.023> (2022).
- Safri, F., Nguyen, R., Zerehpoozheshchi, S., George, J. & Qiao, L. Heterogeneity of hepatocellular carcinoma: from mechanisms to clinical implications. *Cancer Gene Ther.* **31**, 1105–1112. <https://doi.org/10.1038/s41417-024-00764-w> (2024).
- Foglia, B., Turato, C. & Cannito, S. Hepatocellular carcinoma: latest research in pathogenesis, detection and treatment. *Int. J. Mol. Sci.* **24**. <https://doi.org/10.3390/ijms241512224> (2023).
- Ambade, A. et al. Hepatocellular carcinoma is accelerated by NASH involving M2 macrophage polarization mediated by hif-1α-induced IL-10. *Oncoimmunology* **5**, e1221557. <https://doi.org/10.1080/2162402x.2016.1221557> (2016).
- Maas, R. R. et al. The local microenvironment drives activation of neutrophils in human brain tumors. *Cell* **186**, 4546–4566e4527. <https://doi.org/10.1016/j.cell.2023.08.043> (2023).
- Que, H., Fu, Q., Lan, T., Tian, X. & Wei, X. Tumor-associated neutrophils and neutrophil-targeted cancer therapies. *Biochim. Biophys. Acta Rev. Cancer.* **1877**, 188762. <https://doi.org/10.1016/j.bbcan.2022.188762> (2022).
- Zhang, H. et al. Neutrophil, neutrophil extracellular traps and endothelial cell dysfunction in sepsis. *Clin. Transl. Med.* **13**, e1170. <https://doi.org/10.1002/ctm2.1170> (2023).
- Wang, Y., Du, C., Zhang, Y. & Zhu, L. Composition and function of neutrophil extracellular traps. *Biomolecules* **14**. <https://doi.org/10.3390/biom14040416> (2024).
- Song, M. et al. DNA of neutrophil extracellular traps binds TMCO6 to impair CD8 + T-cell immunity in hepatocellular carcinoma. *Cancer Res.* **84**, 1613–1629. <https://doi.org/10.1158/0008-5472.Can-23-2986> (2024).
- Zhan, X. et al. Elevated neutrophil extracellular traps by HBV-mediated S100A9-TLR4/RAGE-ROS cascade facilitate the growth and metastasis of hepatocellular carcinoma. *Cancer Commun. (Lond.)* **43**, 225–245. <https://doi.org/10.1002/cac2.12388> (2023).
- Xia, Y. et al. Neutrophil extracellular traps promote MASH fibrosis by metabolic reprogramming of HSC. *Hepatology*. <https://doi.org/10.1097/hep.0000000000000762> (2024).
- Xin, H. et al. Noninvasive evaluation of neutrophil extracellular traps signature predicts clinical outcomes and immunotherapy response in hepatocellular carcinoma. *Front. Immunol.* **14**, 1134521. <https://doi.org/10.3389/fimmu.2023.1134521> (2023).
- Qu, Z. et al. A novel neutrophil extracellular traps signature for overall survival prediction and tumor microenvironment identification in gastric Cancer. *J. Inflamm. Res.* **16**, 3419–3436. <https://doi.org/10.2147/jir.S417182> (2023).
- Chen, L. et al. Identification and development of an independent immune-related genes prognostic model for breast cancer. *BMC Cancer.* **21**, 329. <https://doi.org/10.1186/s12885-021-08041-x> (2021).
- Love, M. I., Huber, W. & Anders, S. Moderated Estimation of fold change and dispersion for RNA-seq data with DESeq2. *Genome Biol.* **15**, 550. <https://doi.org/10.1186/s13059-014-0550-8> (2014).
- Gustavsson, E. K., Zhang, D., Reynolds, R. H., Garcia-Ruiz, S. & Ryten, M. Ggtranscript: an R package for the visualization and interpretation of transcript isoforms using ggplot2. *Bioinformatics* **38**, 3844–3846. <https://doi.org/10.1093/bioinformatics/btac409> (2022).
- Gu, Z. & Hübschmann, D. Make interactive complex heatmaps in R. *Bioinformatics* **38**, 1460–1462. <https://doi.org/10.1093/bioinformatics/btab806> (2022).
- Hänzelmann, S., Castelo, R. & Guinney, J. GSEA: gene set variation analysis for microarray and RNA-seq data. *BMC Bioinform.* **14**. <https://doi.org/10.1186/1471-2105-14-7> (2013).
- Tian, M. et al. HE4-based nomogram for predicting overall survival in patients with idiopathic pulmonary fibrosis: construction and validation. *Eur. J. Med. Res.* **29**, 238. <https://doi.org/10.1186/s40001-024-01829-0> (2024).
- Langfelder, P. & Horvath, S. WGCNA: an R package for weighted correlation network analysis. *BMC Bioinform.* **9**, 559. <https://doi.org/10.1186/1471-2105-9-559> (2008).
- Yu, G., Wang, L. G., Han, Y. & He, Q. Y. ClusterProfiler: an R package for comparing biological themes among gene clusters. *Omics* **16**, 284–287. <https://doi.org/10.1089/omi.2011.0118> (2012).
- Kanehisa, M., Furumichi, M., Sato, Y., Matsuura, Y. & Ishiguro-Watanabe, M. KEGG: biological systems database as a model of the real world. *Nucleic Acids Res.* **53**, D672–D677 (2025).
- Kanehisa, M. Toward Understanding the origin and evolution of cellular organisms. *Protein Sci.* **28**, 1947–1951 (2019).
- Kanehisa, M. & Goto, S. KEGG: Kyoto encyclopedia of genes and genomes. *Nucleic Acids Res.* **28**, 27–30 (2000).
- Friedman, J., Hastie, T. & Tibshirani, R. Regularization paths for generalized linear models via coordinate descent. *J. Stat. Softw.* **33**, 1–22 (2010).
- Ranganai, E. & Mudhombo, I. Variable selection and regularization in quantile regression via minimum covariance determinant based weights. *Entropy (Basel Switzerland)*. **23**. <https://doi.org/10.3390/e23010033> (2020).
- N'Dilimabaka, N. et al. Biochemical and hematological factors associated with COVID-19 severity among Gabonese patients: A retrospective cohort study. *Front. Cell. Infect. Microbiol.* **12**, 975712. <https://doi.org/10.3389/fcimb.2022.975712> (2022).
- Sachs, M. C. & plotROC A tool for plotting ROC curves. *J. Stat. Softw.* **79**. <https://doi.org/10.18637/jss.v079.c02> (2017).
- Charoentong, P. et al. Pan-cancer Immunogenomic analyses reveal Genotype-Immunophenotype relationships and predictors of response to checkpoint Blockade. *Cell. Rep.* **18**, 248–262. <https://doi.org/10.1016/j.celrep.2016.12.019> (2017).
- Chang, J. et al. Constructing a novel mitochondrial-related gene signature for evaluating the tumor immune microenvironment and predicting survival in stomach adenocarcinoma. *J. Transl. Med.* **21**, 191. <https://doi.org/10.1186/s12967-023-04033-6> (2023).
- Vogel, A., Meyer, T., Sapisochin, G., Salem, R. & Saborowski, A. Hepatocellular carcinoma. *Lancet* **400**, 1345–1362. [https://doi.org/10.1016/s0140-6736\(22\)01200-4](https://doi.org/10.1016/s0140-6736(22)01200-4) (2022).

38. Wang, L. et al. Targeting N6-methyladenosine reader YTHDF1 with SiRNA boosts antitumor immunity in NASH-HCC by inhibiting EZH2-IL-6 axis. *J. Hepatol.* **79**, 1185–1200. <https://doi.org/10.1016/j.jhep.2023.06.021> (2023).
39. Yu, Y. et al. Neutrophil extracellular traps promote immune escape in hepatocellular carcinoma by up-regulating CD73 through Notch2. *Cancer Lett.* **598**, 217098. <https://doi.org/10.1016/j.canlet.2024.217098> (2024).
40. Guo, Z. et al. High expression levels of haem oxygenase-1 promote ferroptosis in macrophage-derived foam cells and exacerbate plaque instability. *Redox Biol.* **76**, 103345. <https://doi.org/10.1016/j.redox.2024.103345> (2024).
41. Karsunky, H., Merad, M., Cozzio, A., Weissman, I. L. & Manz, M. G. Flt3 ligand regulates dendritic cell development from Flt3 + lymphoid and myeloid-committed progenitors to Flt3 + dendritic cells in vivo. *J. Exp. Med.* **198**, 305–313. <https://doi.org/10.1084/jem.20030323> (2003).
42. Grymova, T. et al. Neutrophils are dysregulated in patients with hereditary angioedema types I and II in a Symptom-Free period. *Mediat. Inflamm.* **2019** (9515628). <https://doi.org/10.1155/2019/9515628> (2019).
43. Dong, L. et al. MTOR suppresses cigarette Smoke-Induced airway inflammation and MMP12 expression in macrophage in chronic obstructive pulmonary disease. *Int. J. Chronic Obstr. Pulm. Dis.* **19**, 269–279. <https://doi.org/10.2147/copd.S426333> (2024).
44. Takimoto-Sato, M. et al. Apoptosis inhibitor of macrophage (AIM)/CD5L is involved in the pathogenesis of COPD. *Respir. Res.* **24**, 201. <https://doi.org/10.1186/s12931-023-02508-0> (2023).
45. Saeed, S. et al. Epigenetic programming of monocyte-to-macrophage differentiation and trained innate immunity. *Sci. (New York N Y)*. **345**, 1251086. <https://doi.org/10.1126/science.1251086> (2014).
46. Laidlaw, B. J., Craft, J. E. & Kaech, S. M. The multifaceted role of CD4(+) T cells in CD8(+) T cell memory. *Nat. Rev. Immunol.* **16**, 102–111. <https://doi.org/10.1038/nri.2015.10> (2016).
47. Fonseca, R. et al. Runx3 drives a CD8(+) T cell tissue residency program that is absent in CD4(+) T cells. *Nat. Immunol.* **23**, 1236–1245. <https://doi.org/10.1038/s41590-022-01273-4> (2022).
48. Ma, H. et al. Correction: identification and validation of TNFRSF4 as a high-profile biomarker for prognosis and Immunomodulation in endometrial carcinoma. *BMC cancer.* **22**, 592. <https://doi.org/10.1186/s12885-022-09692-0> (2022).
49. Liu, R. et al. Heme Oxygenase 1 in erythropoiesis: an important regulator beyond catalyzing Heme catabolism. *Ann. Hematol.* **102**, 1323–1332. <https://doi.org/10.1007/s00277-023-05193-7> (2023).
50. Yi, N., Zhang, L., Huang, X., Ma, J. & Gao, J. Lenvatinib-activated NDUFA4L2/IL33/PADI4 pathway induces neutrophil extracellular traps that inhibit Cuproptosis in hepatocellular carcinoma. *Cell. Oncol. (Dordrecht Netherlands)*. <https://doi.org/10.1007/s13402-024-01013-w> (2024).
51. Li, J., Chen, J., Sun, J. & Li, K. The formation of NETs and their mechanism of promoting tumor metastasis. *J. Oncol.* **2023** (7022337). <https://doi.org/10.1155/2023/7022337> (2023).
52. Chen, B. et al. HMOX1 promotes lung adenocarcinoma metastasis by affecting macrophages and mitochondrion complexes. *Front. Oncol.* **12**, 978006. <https://doi.org/10.3389/fonc.2022.978006> (2022).
53. Park, C. S. et al. Can Heme oxygenase-1 be a prognostic factor in patients with hepatocellular carcinoma? *Med. (Baltim)*. **98**, e16084. <https://doi.org/10.1097/md.00000000000016084> (2019).
54. Zheng, C. et al. Donafenib and GSK-J4 synergistically induce ferroptosis in liver Cancer by upregulating HMOX1 expression. *Adv. Sci. (Weinh)*. **10**, e2206798. <https://doi.org/10.1002/adv.202206798> (2023).
55. Gao, M. et al. The deubiquitinase USP7 regulates oxidative stress through stabilization of HO-1. *Oncogene* **41**, 4018–4027. <https://doi.org/10.1038/s41388-022-02403-w> (2022).
56. Yeh, C. N. et al. HO-1 is a favorable prognostic factor for HBV-HCC patients who underwent hepatectomy. *Cancer Manag Res.* **10**, 6049–6059. <https://doi.org/10.2147/cmar.S186931> (2018).
57. Zhong, Y. et al. Small-Molecule Fms-like tyrosine kinase 3 inhibitors: an attractive and efficient method for the treatment of acute myeloid leukemia. *J. Med. Chem.* **63**, 12403–12428. <https://doi.org/10.1021/acs.jmedchem.0c00696> (2020).
58. Kikushige, Y. et al. Human Flt3 is expressed at the hematopoietic stem cell and the granulocyte/macrophage progenitor stages to maintain cell survival. *J. Immunol. (Baltimore Md. : 1950)*. **180**, 7358–7367. <https://doi.org/10.4049/jimmunol.180.11.7358> (2008).
59. Aydin, M. M., Bayin, N. S., Acun, T., Yakicier, M. C. & Akçali, K. C. Role of FLT3 in the proliferation and aggressiveness of hepatocellular carcinoma. *Turk. J. Med. Sci.* **46**, 572–581. <https://doi.org/10.3906/sag-1501-173> (2016).
60. Lai, Y. L., Wang, K. H., Hsieh, H. P. & Yen, W. C. Novel FLT3/AURK multikinase inhibitor is efficacious against sorafenib-refractory and sorafenib-resistant hepatocellular carcinoma. *J. Biomed. Sci.* **29**. <https://doi.org/10.1186/s12929-022-00788-0> (2022).
61. Sun, W. et al. High FLT3 levels May predict Sorafenib benefit in hepatocellular carcinoma. *Clin. Cancer Res.* **26**, 4302–4312. <https://doi.org/10.1158/1078-0432.Ccr-19-1858> (2020).
62. Dobrescu, R., Schipor, S., Manda, D., Caragheorgheopol, A. & Badiu, C. Matrix metalloproteinase-9 (MMP-9) promoter – 1562 C/T functional polymorphism is associated with an increased risk to develop micropapillary thyroid carcinoma. *Cancer Biomark.* **34**, 555–562. <https://doi.org/10.3233/cbm-203119> (2022).
63. Yan, X. L. et al. Hepatocellular carcinoma-associated mesenchymal stem cells promote hepatocarcinoma progression: role of the S100A4-miR155-SOCS1-MMP9 axis. *Hepatol. (Baltimore Md)*. **57**, 2274–2286. <https://doi.org/10.1002/hep.26257> (2013).
64. Cai, N. et al. Targeting MMP9 in CTNNB1 mutant hepatocellular carcinoma restores CD8(+) T cell-mediated antitumour immunity and improves anti-PD-1 efficacy. *Gut* **73**, 985–999. <https://doi.org/10.1136/gutjnl-2023-331342> (2024).
65. Chen, J. et al. Matrix metalloproteinase 9 facilitates hepatitis B virus replication through binding with type I interferon (IFN) receptor 1 to repress IFN/JAK/STAT signaling. *J. Virol.* **91**. <https://doi.org/10.1128/jvi.01824-16> (2017).
66. Yang, C. L. et al. Integrating single-cell and bulk RNA sequencing reveals CK19 + cancer stem cells and their specific SPP1 + tumor-associated macrophage niche in HBV-related hepatocellular carcinoma. *Hepatol. Int.* **18**, 73–90. <https://doi.org/10.1007/s12072-023-10615-9> (2024).
67. Subramanian, S. et al. Indole Curcumin combats metastatic HBV-positive hepatocellular carcinoma by inhibiting cell proliferation, migration, and matrix metalloproteinase-9 activity. *J. Cancer Res. Ther.* **19**, 265–272. https://doi.org/10.4103/jcrt.jcrt_1256_21 (2023).
68. He, M. K. et al. Matrix metalloproteinase 12 expression is associated with tumor FOXP3(+) regulatory T cell infiltration and poor prognosis in hepatocellular carcinoma. *Oncol. Lett.* **16**, 475–482. <https://doi.org/10.3892/ol.2018.8642> (2018).
69. Elshimi, E., Sakr, M. A. M., Morad, W. S. & Mohammad, L. Optimizing the diagnostic role of Alpha-Fetoprotein and abdominal ultrasound by adding overexpressed blood mRNA matrix Metalloproteinase-12 for diagnosis of HCV-Related hepatocellular carcinoma. *Gastrointest. Tumors.* **5**, 100–108. <https://doi.org/10.1159/000495838> (2019).
70. Guo, Z. Y. & Jiang, L. P. Matrix metalloproteinase 12 (MMP12) as an adverse prognostic biomarker of vascular invasion in hepatic cell carcinoma. *Eur. Rev. Med. Pharmacol. Sci.* **26**, 2238–2249. https://doi.org/10.26355/eurev_202204_28454 (2022).
71. Gao, H. et al. Role of matrix metalloproteinase 12 in the development of hepatocellular carcinoma. *J. Invest. Surg.* **34**, 366–372. <https://doi.org/10.1080/08941939.2019.1637975> (2021).
72. Cong, T. et al. The role of GNMT and MMP12 expression in determining TACE efficacy: validation at transcription and protein levels. *J. Hepatocell Carcinoma.* **11**, 95–111. <https://doi.org/10.2147/jhc.S441179> (2024).
73. Li, N. et al. Deficient DNASE1L3 facilitates neutrophil extracellular traps-induced invasion via Cyclic GMP-AMP synthase and the non-canonical NF-κB pathway in diabetic hepatocellular carcinoma. *Clin. Translational Immunol.* **11**, e1386. <https://doi.org/10.1002/cti2.1386> (2022).
74. Fan, G. et al. Single-cell and Spatial analyses revealed the co-location of cancer stem cells and SPP1 + macrophage in hypoxic region that determines the poor prognosis in hepatocellular carcinoma. *NPJ Precision Oncol.* **8**. <https://doi.org/10.1038/s41698-024-00564-3> (2024).

75. Croft, M. et al. OX40 in the pathogenesis of atopic Dermatitis-A new therapeutic target. *Am. J. Clin. Dermatol.* **25**, 447–461. <https://doi.org/10.1007/s40257-023-00838-9> (2024).
76. Wang, D. et al. Elevated expression of TNFRSF4 impacts immune cell infiltration and gene mutation in hepatocellular carcinoma. *Cancer Biomark. A.* **36**, 147–159. <https://doi.org/10.3233/cbm-210538> (2023).
77. Yan, Z., Li, X., Li, Z., Liu, S. & Chang, H. Prognostic significance of TNFRSF4 expression and development of a pathomics model to predict expression in hepatocellular carcinoma. *Heliyon* **10**, e31882. <https://doi.org/10.1016/j.heliyon.2024.e31882> (2024).
78. Zhou, Z. et al. The combination immunotherapy of TLR9 agonist and OX40 agonist via intratumoural injection for hepatocellular carcinoma. *J. Hepatocell Carcinoma* **8**, 529–543. <https://doi.org/10.2147/jhc.S301375> (2021).
79. Zhao, M. et al. Cytochrome P450 enzymes and drug metabolism in humans. *Int. J. Mol. Sci.* **22**. <https://doi.org/10.3390/ijms222312808> (2021).
80. Ishteyaque, S., Yadav, K. S., Verma, S., Washimkar, K. R. & Mugale, M. N. CYP2E1 triggered GRP78/ATF6/CHOP signaling axis inhibit apoptosis and promotes progression of hepatocellular carcinoma. *Arch. Biochem. Biophys.* **745**, 109701. <https://doi.org/10.1016/j.abb.2023.109701> (2023).
81. Yang, K. L. et al. Axitinib in combination with radiotherapy for advanced hepatocellular carcinoma: a phase I clinical trial. *Radiat. Oncol.* **16**, 18. <https://doi.org/10.1186/s13014-020-01742-w> (2021).
82. Donne, R. & Lujambio, A. The liver cancer immune microenvironment: therapeutic implications for hepatocellular carcinoma. *Hepatology* **77**, 1773–1796. <https://doi.org/10.1002/hep.32740> (2023).
83. Zhang, A. et al. Regulatory T cells in immune checkpoint Blockade antitumor therapy. *Mol. Cancer* **23**, 251. <https://doi.org/10.1186/s12943-024-02156-y> (2024).
84. Scott, E. N., Gocher, A. M., Workman, C. J. & Vignali, D. A. A. Regulatory T cells: barriers of immune infiltration into the tumor microenvironment. *Front. Immunol.* **12**, 702726. <https://doi.org/10.3389/fimmu.2021.702726> (2021).
85. Gao, X. et al. Immunotherapy targeting Myeloid-Derived suppressor cells (MDSCs) in tumor microenvironment. *Front. Immunol.* **11**, 585214. <https://doi.org/10.3389/fimmu.2020.585214> (2020).
86. Li, M. et al. Spatial proteomics of immune microenvironment in nonalcoholic steatohepatitis-associated hepatocellular carcinoma. *Hepatology* **79**, 560–574. <https://doi.org/10.1097/hep.0000000000000591> (2024).
87. Lu, L. C., Chang, C. J. & Hsu, C. H. Targeting myeloid-derived suppressor cells in the treatment of hepatocellular carcinoma: current state and future perspectives. *J. Hepatocell Carcinoma* **6**, 71–84. <https://doi.org/10.2147/jhc.S159693> (2019).
88. Wang, W., Li, J., Pan, C., Wang, D. & Dong, J. miR-328-3p suppresses hepatocellular carcinoma progression by regulating HMOX1 expression. *Discover Oncol.* **15**, 735. <https://doi.org/10.1007/s12672-024-01610-z> (2024).
89. Li, Z. et al. Association of CXCR1 and 2 expressions with gastric cancer metastasis in ex vivo and tumor cell invasion in vitro. *Cytokine* **69**, 6–13. <https://doi.org/10.1016/j.cyto.2014.05.004> (2014).
90. Liu, L., Zhang, W., Hu, Y., Ma, L. & Xu, X. Downregulation of miR-1225-5p is pivotal for proliferation, invasion, and migration of HCC cells through NFκB regulation. *J. Clin. Lab. Anal.* **34**, e23474. <https://doi.org/10.1002/jcla.23474> (2020).
91. Iwata, T. et al. PD-L1(+)MDSCs are increased in HCC patients and induced by soluble factor in the tumor microenvironment. *Sci. Rep.* **6**, 39296. <https://doi.org/10.1038/srep39296> (2016).
92. Liu, G. et al. M2 macrophages promote HCC cells invasion and migration via miR-149-5p/MMP9 signaling. *J. Cancer* **11**, 1277–1287. <https://doi.org/10.7150/jca.35444> (2020).
93. Zhou, X. et al. Macrophage-derived MMP12 promotes fibrosis through sustained damage to endothelial cells. *J. Hazard. Mater.* **461**. <https://doi.org/10.1016/j.jhazmat.2023.132733> (2024).
94. Carow, C. E. et al. Expression of the hematopoietic growth factor receptor FLT3 (STK-1/Flk2) in human leukemias. *Blood* **87**, 1089–1096 (1996).
95. Li, K. et al. Myeloid-derived suppressor cells as immunosuppressive regulators and therapeutic targets in cancer. *Signal. Transduct. Target. Therapy* **6**. <https://doi.org/10.1038/s41392-021-00670-9> (2021).
96. Lin, D. et al. Development and validation of a nomogram to evaluate the therapeutic effects of second-line axitinib in patients with metastatic renal cell carcinoma. *Front. Oncol.* **13**, 1071816. <https://doi.org/10.3389/fonc.2023.1071816> (2023).
97. Sánchez-Díez, M. et al. Assessment of cell viability in drug therapy: IC50 and other new Time-Independent indices for evaluating chemotherapy efficacy. *Pharmaceutics* **17**. <https://doi.org/10.3390/pharmaceutics17020247> (2025).
98. He, J., Huang, Z., Han, L., Gong, Y. & Xie, C. Mechanisms and management of 3rd-generation EGFR-TKI resistance in advanced non-small cell lung cancer (Review). *Int. J. Oncol.* **59**. <https://doi.org/10.3892/ijo.2021.5270> (2021).
99. Bai, Z. et al. Identification and Validation of Cuproptosis-Related LncRNA Signatures in the Prognosis and Immunotherapy of Clear Cell Renal Cell Carcinoma Using Machine Learning. *Biomolecules* **12**. <https://doi.org/10.3390/biom12121890> (2022).

Acknowledgements

We would like to express our sincere gratitude to all individuals and organizations who supported and assisted us throughout this research.

Author contributions

Material preparation, data collection and analysis were performed by Yuan Defeng, Zhang Zhengcong, Zhang Feng, Lv Pengfei, Zhu Jun and Zhang Haiwei. The first draft of the manuscript was written by Yuan Defeng. All authors reviewed the manuscript.

Funding

This work was supported by the Natural Science Foundation of Gansu Province (Grant No. 21JR11RA080) and the University Teachers Innovation Fund Project of Gansu Province (Grant No. 2023B-002).

Declarations

Competing interests

The authors declare no competing interests.

Ethical approval

This study was performed in line with the principles of the Declaration of Helsinki. Approval was granted by the Medical Ethics Committee of the First Hospital of Lanzhou University (LDYLL2024-759).

Consent to participate

Informed consent was obtained from all individual participants included in the study.

Additional information

Supplementary Information The online version contains supplementary material available at <https://doi.org/10.1038/s41598-025-01335-1>.

Correspondence and requests for materials should be addressed to Z.Z.

Reprints and permissions information is available at www.nature.com/reprints.

Publisher's note Springer Nature remains neutral with regard to jurisdictional claims in published maps and institutional affiliations.

Open Access This article is licensed under a Creative Commons Attribution-NonCommercial-NoDerivatives 4.0 International License, which permits any non-commercial use, sharing, distribution and reproduction in any medium or format, as long as you give appropriate credit to the original author(s) and the source, provide a link to the Creative Commons licence, and indicate if you modified the licensed material. You do not have permission under this licence to share adapted material derived from this article or parts of it. The images or other third party material in this article are included in the article's Creative Commons licence, unless indicated otherwise in a credit line to the material. If material is not included in the article's Creative Commons licence and your intended use is not permitted by statutory regulation or exceeds the permitted use, you will need to obtain permission directly from the copyright holder. To view a copy of this licence, visit <http://creativecommons.org/licenses/by-nc-nd/4.0/>.

© The Author(s) 2025